

Accepted for publication in the *Astrophysical Journal* on 2010
September 13.

FARADAY ROTATION IN THE TAIL OF THE PLANETARY NEBULA DeHt 5

R. R. Ransom^{1,2}, R. Kothes², M. Wolleben² and T. L. Landecker²

RRansom@okanagan.bc.ca

ABSTRACT

We present 1420 MHz polarization images of a $5^\circ \times 5^\circ$ region around the planetary nebula (PN) DeHt 5. The images reveal narrow Faraday-rotation structures on the visible disk of DeHt 5, as well as two wider, tail-like, structures “behind” DeHt 5. Though DeHt 5 is an old PN known to be interacting with the interstellar medium (ISM), a tail has not previously been identified for this object. The innermost tail is ~ 3 pc long and runs away from the north-east edge of DeHt 5 in a direction roughly opposite that of the sky-projected space velocity of the white dwarf central star, WD 2218+706. We believe this tail to be the signature of ionized material ram-pressure stripped and deposited downstream during a $>74,000$ yr interaction between DeHt 5 and the ISM. We estimate the rotation measure (RM) through the inner tail to be -15 ± 5 rad m⁻², and, using a realistic estimate for the line-of-sight component of the ISM magnetic field around DeHt 5, derive an electron density in the inner tail of $n_e = 3.6 \pm 1.8$ cm⁻³. Assuming the material is fully ionized, we estimate a total mass in the inner tail of 0.68 ± 0.33 M_⊙, and predict that 0.49 ± 0.33 M_⊙ was added during the PN-ISM interaction. The outermost tail consists of a series of three roughly circular components, which have a collective length of ~ 11.0 pc. This tail is less conspicuous than the inner tail, and may be the signature of the earlier interaction between the WD 2218+706 asymptotic giant branch (AGB) progenitor and the ISM. The results for the inner and outer tails are consistent with hydrodynamic simulations, and may have implications for the PN missing-mass problem as well

¹Department of Physics and Astronomy, Okanagan College, 583 Duncan Avenue West, Penticton, B.C., V2A 8E1, Canada

²National Research Council of Canada, Herzberg Institute of Astrophysics, Dominion Radio Astrophysical Observatory, Box 248, Penticton, BC, V2A 6J9, Canada

as for models which describe the impact of the deaths of intermediate-mass stars on the ISM.

Subject headings: planetary nebulae: individual (DeHt 5) — ISM: structure — polarization — radio continuum: ISM

1. INTRODUCTION

Interaction with the interstellar medium (ISM) is expected for planetary nebulae (PNe) in a later stage of evolution (e.g., Borkowski, Sarazin, & Soker 1990). In the early stages, the shell of the PN (i.e., the region where the fast wind from the hot central star collides with the slow wind from its progenitor) has high density, and the PN expands essentially unimpeded into the surrounding ISM. As the nebula expands, its density decreases, and at some point the thermal pressure in the nebular shell drops to a value equal to the ram pressure of the ISM. In many cases, the magnetic pressure from the magnetized ISM should also be considered (e.g., Soker & Dgani 1997). Equal internal and external pressures mark the proposed start of the PN-ISM interaction. Since all stars have some peculiar motion, and the ISM pressure is proportional to the square of the speed of the PN system relative to the ambient ISM, the PN-ISM interaction appears first as a bow shock upstream from the central star. Indeed, an asymmetric emission structure is the observational marker for PN-ISM interaction in old PNe with large proper motions (Tweedy & Kwitter 1996; Xilouris et al. 1996; Kerber et al. 2000).

Recently, two-dimensional (Villaver, García-Segura, & Manchado 2003) and three dimensional (Wareing et al. 2006b; Wareing, Zijlstra, & O’Brien 2007a; Wareing et al. 2007c) hydrodynamic simulations have been used to show that the interaction between an evolved intermediate-mass star ($\sim 1\text{--}7\text{ M}_{\odot}$) and the ISM likely starts during the asymptotic giant branch (AGB) stage. The simulations predict that for any system moving with respect to the ambient (warm neutral or warm ionized) ISM, an upstream bow shock is formed between the slow, dense AGB wind and the ISM. Additionally, the simulations predict that material is ram-pressure stripped from the upstream interface and deposited downstream to form a comet-like tail behind the moving system. These predictions are confirmed for at least one star, namely the primary (AGB) star in the Mira AB binary (see Martin et al. 2007; Matthews et al. 2008). Far-ultraviolet observations for this high-proper-motion system show emission from both a bow shock and a $\sim 4\text{-pc}$ -long tail (Martin et al. 2007).

The simulations of Wareing et al. (2006b, 2007a) further predict that the AGB-ISM bow shock shapes the PN expansion during the later stages of PN evolution, and in fact

describes the PN-ISM interaction, not as an interaction between the expanding PN shell and the ISM, but rather a collision between the PN shell and the pre-existing AGB-ISM bow shock. This PN-AGB-ISM interaction scenario (also called the “triple wind” model) works very well to explain the general shaping of many PN displaying characteristics of ISM interaction (Wareing et al. 2007a). Moreover, for one of the more prominent examples of ISM interaction, PN Sh 2-188, simulations are able to reproduce the observed structure and brightness distribution, and predict both the time scale for the interaction and (with the proper motion of the central star yet undetermined) the relative speed of the system through the ISM (Wareing et al. 2006a).

In addition to the predictions and apparent successes of the triple-wind model described above, Wareing et al. (2007a) (and previously Villaver et al. 2003) suggest that the model may also solve the “missing-mass” problem in PNe, whereby only a small fraction of the mass ejected during the AGB phase is observed to be present (in ionized form) during the PN phase (see, e.g., Zhang 1995). The simulations of Villaver et al. and Wareing et al. suggest that during the relatively long AGB phase, a large fraction ($\gtrsim 60\%$) of the expelled mass is stripped at the AGB-ISM interface and deposited downstream. Moreover, this process appears to be important for systems moving near the Galactic plane at even modest speeds with respect to the ISM. The detections so far of tails behind an AGB star, Mira AB, and two PN systems, Sh 2-188 and Sh 2-68 (see Xilouris et al. 1996; Kerber et al. 2002), suggest that intermediate-mass stars distribute mass over much larger volumes than predicted for PN expansion alone. Finding other tails and, more importantly, estimating the total mass present in a tail, is thus an important next step in quantifying the degree to which these stars spread processed material throughout the ISM.

The surface brightnesses of the tails behind Mira AB, Sh 2-188, and Sh 2-68 are very low. For the two PNe, the tail emission was detected with deep $H\alpha$ observations, while for Mira AB, the ~ 4 -pc-tail emission was detected with deep, narrow-band ultraviolet observations. Surveys in $H\alpha$ may, if carefully perused, reveal other tails. However, it is unlikely that they can be used to trace the full mass-loss histories of interacting systems, since the material stripped during the AGB phase will be very diffuse and at least partially deionized. On the other hand, the ultraviolet emission in the Mira AB tail, though tracing a significant fraction of the mass-loss period for that system, suggests an unusual, and perhaps unique, emission mechanism. Recent observations of the neutral component in the Mira AB tail suggest that H I imaging is a useful tool for studying the morphology and dynamics of tails behind evolved stars, but high-resolution H I images may be limited to the densest (i.e., innermost) regions of the tails. A better tool for locating and studying the extended tails behind evolved intermediate-mass stars may be radio polarimetric observations. Polarimetric observations at frequencies ≤ 3 GHz (wavelengths ≥ 10 cm) are very sensitive to Faraday

rotation of the diffuse Galactic synchrotron emission (e.g., Uyaniker et al. 2003), and have been used previously to study the interaction region at the upstream interface between PN Sh 2-216 and the ISM (Ransom et al. 2008). In propagating through the magnetized ISM, the polarized component of the background emission is rotated at wavelength λ [m] through an angle

$$\Delta\theta = RM \lambda^2 \text{ [rad]}, \quad (1)$$

where RM is the rotation measure and depends on the line-of-sight component of the magnetic field, B_{\parallel} [μ G], the thermal electron density, n_e [cm^{-3}], and the path length, dl [pc], as

$$RM = 0.81 \int B_{\parallel} n_e dl \text{ [rad m}^{-2}\text{]}. \quad (2)$$

Even in the relatively low electron-density environment expected in the tail behind a PN or AGB star ($n_e \approx n_H \sim 1 \text{ cm}^{-3}$, see Wareing et al. 2007a), a rotation of the background polarization angle of $\Delta\theta \sim 5^\circ$ can be expected for a system moving through the ISM near the Galactic plane.¹ Such a rotation will result in a Faraday-rotation signature for the tail which is readily observable, albeit one which can be corrupted by other, perhaps more turbulent, structures along the line of sight.

In this paper, we report the discovery of a Faraday-rotation structure consistent with a tail behind the fast-moving PN DeHt 5 (=DHW 5; PK 111.0+11.6). The structure is identified in the 1420 MHz polarization images of the Canadian Galactic Plane Survey (CGPS). DeHt 5 is an old PN known to be interacting with the ISM (Tweedy & Kwitter 1996), but no tail has previously been associated with this object. In § 2.1, we summarize the properties of DeHt 5, and compute its space velocity relative to the local ISM. In § 3, we describe briefly the preparation of the CGPS polarization images for the region surrounding DeHt 5. In § 4, we characterize the Faraday-rotation structures at the position of DeHt 5 and in the tail behind DeHt 5, and estimate the RM s through the inner and outer portions of the tail. In § 5, we discuss in detail the PN and tail structures, and estimate the electron densities, and thus hydrogen-mass densities, in the inner and outer tails. Finally, in § 6, we give a summary of our results and present our conclusions.

¹We assume for the calculation of $\Delta\theta$ an observing frequency of 1420 MHz ($\lambda = 21 \text{ cm}$), i.e., the principal frequency of the Galactic Plane Surveys (e.g., Landecker et al. 2010; Haverkorn et al. 2006), and use values of $2 \mu\text{G}$ and 1 pc for the line-of-sight component of the Galactic magnetic field and the path length through the tail, respectively.

2. THE PLANETARY NEBULA DeHt 5

DeHt 5 is an old PN (see Table 1) whose optical morphology clearly demonstrates interaction with the ISM. Indeed, the narrow-band and emission-line images of Tweedy & Kwitter (1996) show that the intrinsic morphology of the PN may have been largely destroyed by the PN-ISM interaction. For point of illustration, we show in Figure 1 the Digitized Sky Survey (DSS) R-band ($\lambda = 657\text{ nm}$) optical image for the $1^\circ \times 1^\circ$ region centered on the DeHt 5 white dwarf central star, WD 2218+706. The brightest and most distinct portion of the PN is marked by the filamentary emission to the (Galactic) north of WD 2218+706. The remainder of the PN is significantly more diffuse and amorphous. The $9'$ -diameter dashed circle in Figure 1 (and in subsequent figures featuring the radio polarization images) represents the approximate visible extent of DeHt 5 (see Tweedy & Kwitter 1996), and, for lack of a better reference point, is centered on WD 2218+706. We emphasize, however, that the “visible disk” of DeHt 5 has neither a distinct circular shape nor is it necessarily centered on WD 2218+706. In fact, given the age of DeHt 5, it is very likely that WD 2218+706 is offset from the center of the PN in the direction of motion. We therefore advise the reader to use the disk outline as it appears in each figure only as a rough guide to the size and position of DeHt 5.

2.1. Space Velocity of DeHt 5

We can use the parallax, proper motion, and radial velocity of WD 2218+706 (see Table 1) to estimate the UVW motion of DeHt 5 through the ISM, where the U component is positive toward the Galactic center, V is positive in the direction of Galactic rotation, and W is positive toward the north Galactic pole (e.g., Johnson & Soderblom 1987). After correcting for a solar motion of $(U_\odot, V_\odot, W_\odot) = (10.00 \pm 0.36, 5.25 \pm 0.62, 7.17 \pm 0.38) \text{ km s}^{-1}$ (Dehnen & Binney 1998), we find velocity components for WD 2218+706 of $(U, V, W) = (+54.18 \pm 1.28, -18.14 \pm 3.38, -15.39 \pm 0.81) \text{ km s}^{-1}$. The overall space velocity of DeHt 5 through the ambient² ISM is then $59.17 \pm 3.70 \text{ km s}^{-1}$, with components on the sky and along the line of sight of $45.8 \pm 2.4 \text{ km s}^{-1}$ and $37.5 \pm 3.2 \text{ km s}^{-1}$, respectively. The sky-projected space velocity of DeHt 5, including error cone, is illustrated in Figure 1 (optical image) as well as Figures 2 and 3 (radio polarization images).

The space velocity of DeHt 5 is consistent with the average value ($\sim 60 \text{ km s}^{-1}$) given

²We do not take into account any motion from an interstellar cloud that may contain DeHt 5. If DeHt 5 is indeed part of a cloud, then the quoted space velocity may be off by up to $\sim 5 \text{ km s}^{-1}$ (see Bannister et al. 2001).

by Borkowski et al. (1990) for Galactic disk PNe. To better establish its population membership, we integrated the Galactic orbital motion of DeHt 5 using the initial velocity components given above and the Galactic gravitational potential derived by Dauphole & Colin (1995). We do not plot the results, but note that the orbit of DeHt 5 is confined to within 200 pc of the Galactic plane, indicating that DeHt 5 is a thin disk PN. We discuss the trajectory of DeHt 5 over the last ~ 2 Myr in § 5.2.

3. OBSERVATIONS AND IMAGE PREPARATION

The radio polarization data presented in this paper were obtained at 1420 MHz ($\lambda = 21$ cm) as part of the CGPS (Taylor et al. 2003). The particular area of interest actually falls in the high-latitude extension of the CGPS: a region between Galactic longitudes $l = 100^\circ$ and $l = 117^\circ$ for which the nominal coverage in Galactic latitude (i.e., $-3.6^\circ < b < +5.6^\circ$) is increased to $-3.6^\circ < b < +17.5^\circ$ (see Landecker et al. 2010). The principal observing instrument for the radio component of the CGPS is the synthesis telescope (ST; see Landecker et al. 2000) at the Dominion Radio Astrophysical Observatory (DRAO). The ST collects continuum data in four 7.5 MHz bands centered on 1406.65, 1414.15, 1426.65 and 1434.15 MHz, respectively.³ The ST is sensitive at 1420 MHz to emission from structures with angular sizes of $\sim 1^\circ$ down to the resolution limit of $\sim 1'$. In Stokes-Q (Q) and Stokes-U (U), data from two single-antenna surveys of the northern sky at ~ 1.4 GHz, namely the DRAO-26m survey (Wolleben et al. 2006) and the Effelsberg Medium Latitude Survey (Reich et al. 2004), are added to the band-averaged ST data to provide information on the largest spatial scales (see Landecker et al. 2010).

CGPS data calibration and processing procedures are described in detail in Taylor et al. (2003). A summary of the specific procedures used to calibrate the polarization data is given in Ransom et al. (2008). The estimated noise level in the band-averaged images produced for the $5^\circ \times 5^\circ$ region of the CGPS presented in this paper is ~ 0.34 mJy beam $^{-1}$ (~ 0.045 K).

³Note that the frequency corresponding to the midpoint of the four continuum bands is 1420.4 MHz, the neutral hydrogen spin-flip frequency. The 5.0 MHz band about this frequency is allocated to the 256-channel spectrometer (see Taylor et al. 2003).

4. RADIO POLARIZATION IMAGES OF PN DeHt 5

In Figure 2 we show the polarized intensity ($P = \sqrt{Q^2 + U^2 - (1.2\sigma)^2}$; e.g., Simmons & Stewart 1985), where the last term gives explicitly the noise bias correction) and polarization angle ($\theta_P = \frac{1}{2} \arctan U/Q$) images at 1420 MHz ($\lambda = 21$ cm) for the $1^\circ \times 1^\circ$ region about DeHt 5 (i.e., the same region presented optically in Figure 1). The images reveal narrow polarization structures on and immediately (to the Galactic) north-east of the visible disk of the PN, as well as an extended polarization structure which runs east-northeast from the edge of the visible disk to the edge of the displayed region. (Recall, visible disk, or “disk” as it is shortened to hereafter, refers to the approximate visible extent of DeHt 5; see § 2.) The reduced intensity of these structures, compared to the relatively smooth polarized emission in all other parts of the $1^\circ \times 1^\circ$ region, indicates that their appearances are due to the effects of Faraday rotation; namely localized beam depolarization of the background diffuse synchrotron emission and/or background-foreground cancellation (e.g., Gray et al. 1999). The coincidence of the narrow structures with the disk of DeHt 5 suggests that their origin is the shell of the PN (see § 4.1).

To better characterize structures outside the disk of the PN, we show in Figure 3 the polarized intensity and polarization angle images for a $5^\circ \times 5^\circ$ region about DeHt 5. The extended Faraday-rotation structure, noted above, is the most distinct feature in the region. It is $\sim 0.5^\circ$ long and $\sim 0.3^\circ$ wide, with a major-axis position angle (p.a.) of $\sim 32^\circ$ (north of east). The major axis of the structure is nearly (counter-)aligned with the projected space velocity of DeHt 5 (p.a. = $10.5^\circ \pm 2.5^\circ$, south of west), suggesting that the origin of this structure may be a tail (labeled “thick tail” in Figure 3) of ionized material deposited downstream from the PN. We estimate the RM of the thick tail in § 4.2, and provide evidence for its physical association with DeHt 5 in § 5.2. If we track north-east from the easternmost edge of this tail-like structure, we encounter three additional, though more subtle, Faraday-rotation structures (labeled “thin tail” in Figure 3) along roughly the same line. We estimate the mean RM of these structures in § 4.3, and speculate on their origin in § 5.2.

We do not believe any of the remaining polarization structures in Figure 3 are associated with DeHt 5. The filamentary structure immediately south-east of DeHt 5 (see also Figure 1) is coincident with optical filaments described by Bally & Reipurth (2001) and considered by them to be part of supernova remnant (SNR) G110.3+11.3.

4.1. Faraday-Rotation on the Disk of DeHt 5

Figure 2a and a close-up view in Figure 4a show a low-polarized-intensity ridge which runs approximately east-to-west through the projected center of DeHt 5, and a low-polarized-intensity arc which approximately traces the north-east edge of DeHt 5. The mean polarized intensities for the ridge and arc are 0.103 ± 0.044 K and 0.081 ± 0.039 K, respectively, or ~ 0.35 and ~ 0.27 times the off-source value of 0.297 ± 0.047 K (see Table 2). In addition, each of these structures has small beam-sized (i.e., $\sim 1'$ -diameter) areas for which the polarized intensities are virtually zero. The low mean intensities and small-scale spatial variations in both the ridge and arc point to beam depolarization (rather than background/foreground cancellation) as the dominant depolarization mechanism in these structures. Moreover, beam depolarization is consistent with the Faraday rotation for the ridge and arc occurring in the shell of DeHt 5: sharp RM gradients are caused by fluctuations (in projected position on the sky) in either electron density or line-of-sight magnetic field strength (see Equation 2), each of which is expected in the turbulent shell of a PN (e.g., Ransom et al. 2008).

Figure 2b and a close-up view in Figure 4b show that the polarization angles for the ridge and arc are significantly rotated compared to the off-source value of $-48^\circ \pm 6^\circ$ (see Table 2). Moreover, the polarization angles at the outside edges of the ridge and arc (white or near-white pixels) appear to outline a single “bent” structure with clear boundaries on the north-east side (arc) and south side (ridge). At approximately the midpoint between the arc and ridge (see Figure 4), the polarization angles plateau at $-29^\circ \pm 9^\circ$, a value different from that seen both off-source (i.e., north-west, west, and south of the disk) and in the thick tail immediately north-east of the arc (see Table 2). Compared to the off-source value, the mean polarization angle in the “plateau” is rotated $+19^\circ \pm 11^\circ$. We infer positive, i.e., counter-clockwise, rotation, since the alternative, namely a negative rotation of $\sim -161^\circ$, would likely produce a clear (black-to-white) boundary in polarization angle at the north and north-west edges of the disk. No such boundary is seen. Also, the polarization angles in our four ST bands (see § 3) do not reflect a $RM \sim 9$ times larger than that derived below for the (smaller) positive rotation. (Rotations corresponding to additional positive or negative 180° “wraps” in polarization angle are excluded by the data.) The mean polarized intensity over the plateau is 0.252 ± 0.045 K, a very modest reduction from the off-source value, which suggests for this small region that background/foreground cancellation is more important than beam depolarization. If we assume that the Faraday rotation takes place in the shell of DeHt 5, i.e., at a distance of 345 ± 20 pc, and use the values for the foreground polarized intensity and polarization angle given in § 4.2 for the line of sight toward the thick tail, we estimate by comparing off-source and on-source polarization angles a mean RM over the plateau region of $+18 \pm 12$ rad m $^{-2}$. We comment on the viability of using on-source/off-source polarization angles to estimate RM s in § 4.2.

The most prominent polarization structures on (or near) the disk of DeHt 5 (i.e., the ridge and arc) do not coincide spatially with the bright filamentary structure seen in optical emission (Figure 1) at the north edge of DeHt 5. Nevertheless, we believe that the approximate confinement of the ridge and plateau region to the disk of DeHt 5 and close correspondence between the arc and the north-east edge of the disk provide strong evidence that each structure (or single common structure) is physically associated with the shell of the PN. We elaborate on the physical association in more detail in § 5.1.

4.2. Faraday-Rotation in the Thick Tail

The $\sim 0.5^\circ \times \sim 0.3^\circ$ thick tail (see Figures 2 and 3) stands out noticeably in both polarized intensity and polarization angle relative to the (off-source) region near DeHt 5. The 0.162 ± 0.055 K mean polarized intensity in the thick tail is ~ 0.55 times the off-source value of 0.297 ± 0.047 K, and the $-72^\circ \pm 8^\circ$ mean polarization angle is rotated $\sim -24^\circ$ compared to the off-source value of $-48^\circ \pm 6^\circ$ (see Table 2). A negative, i.e., clockwise, rotation makes sense, given the absence of sharp polarized-intensity and polarization-angle boundaries at the edge of the thick tail, and is supported by our Faraday-rotation models (see below). While the reduction in mean intensity is more modest for the thick tail than for the narrow features on the disk of DeHt 5, small beam-sized “knots” of near-zero polarized intensity and rapid polarization-angle variation indicate the presence of sharp, localized RM gradients in the thick tail. As with the ridge and arc, beam depolarization probably defines the knots.

If we exclude the knots, the mean polarized intensity in the thick tail increases slightly to 0.182 ± 0.039 K, or ~ 0.61 times the off-source value. The mean polarization angle is $-66^\circ \pm 6^\circ$, a rotation of $-18^\circ \pm 8^\circ$ from the off-source value. The $\sim 39\%$ reduction in the polarized intensity compared to that off-source, and relatively small standard deviations about the mean values in polarized intensity and polarization angle (compared the ridge and arc), suggest that, outside of the knots, background/foreground cancellation is of comparable importance to beam depolarization. We constructed Faraday-rotation models using the approach of Wolleben & Reich (2004). We treated the thick tail (excluding the knots) as a Faraday “screen” that rotates the polarization angle of the background emission. When the rotated background is vector-added to the polarized foreground, the net polarized intensity drops (compared to regions outside of the screen). For each model, we varied the RM and degree of beam depolarization for the screen as well as the foreground polarized intensity and polarization angle. Our set of acceptable models (judged against the scatter in the on-source and off-source data) gives a RM over the thick tail of -15 ± 5 rad m $^{-2}$. The models

also give a foreground polarized intensity of 0.160 ± 0.050 K and foreground polarization angle of $-45^\circ \pm 10^\circ$, and indicate that beam depolarization accounts for $40\% \pm 10\%$ of the intensity reduction in the thick tail. The foreground polarized intensity is consistent with the 0.12–0.23 K value suggested by Roger et al. (1999) for the 345 ± 20 pc line of sight toward DeHt 5.⁴ Note that the polarization angle is very similar to the nominal off-source value.

Estimating RM s by comparing on-source and off-source polarization angles is subject to rather large uncertainties, particularly when the foreground toward the source of interest contributes a significant fraction of the polarized emission ($\gtrsim 50\%$). While we believe that the value quoted above for the thick tail is accurate within the uncertainties, a direct estimate of the RM using (widely spaced) multi-frequency polarimetric data would be superior. Future polarimetric observations at subarcminute resolution and at multiple frequencies in the 1–3 GHz range could provide a detailed RM -map of the region around DeHt 5.

4.3. Faraday-Rotation in the Thin Tail

The less conspicuous thin tail (see Figure 3) is comprised of three Faraday-rotation structures, each roughly $\sim 0.3^\circ$ in diameter, and has a total length of $\sim 1.8^\circ$. The mean polarized intensity across all three structures is 0.260 ± 0.048 , or ~ 0.84 times the off-source value for the region around the thin tail of 0.309 ± 0.047 K (see Table 2). The mean polarization angle across all three structures is $-55^\circ \pm 6^\circ$, a rotation of $-7^\circ \pm 8^\circ$ from the off-source value of $-48^\circ \pm 6^\circ$ (see Table 2).⁵ We again infer a negative rotation, since there are no sharp boundaries at the edges of these structures. If we assume that the Faraday rotation takes place at a distance of 345 ± 20 pc, and use the values for the foreground polarized intensity and polarization angle given in § 4.2 for the line of sight toward the thick

⁴Roger et al. (1999) give emissivity measurements at 22 MHz for lines of sight near DeHt 5. Reich & Reich (1988) show that the brightness temperature spectral index between 408 and 1420 MHz for the region around DeHt 5 is $\beta = -2.7$ ($T_B \sim \nu^\beta$). If we assume that this value applies also to the frequency range 22–408 MHz, then (assuming the emission is $\approx 70\%$ polarized) the Roger et al. measurements give a foreground polarized intensity of 0.125 ± 0.010 K. However, low-angular-resolution maps between 38 and 408 MHz suggest a slightly flatter index ($\beta = -2.5$; Lawson et al. 1987) at lower frequencies. Applying $\beta = -2.5$ between 22 and 408 MHz and $\beta = -2.7$ between 408 and 1420 MHz, the Roger et al. measurements give a foreground polarized intensity of 0.215 ± 0.015 K.

⁵Though roughly consistent with zero, the $-7^\circ \pm 8^\circ$ on-source/off-source rotation nevertheless yields thin-tail structures which stand out in contrast relative to the smoother off-source regions. The true standard error for the rotation is likely smaller than 8° (computed as the root-sum-square of the standard deviations of the polarization angles for the thin tail and off-source region), but is difficult to estimate in the absence of a Faraday-rotation model.

tail, we estimate by comparing off-source and on-source polarization angles a mean RM over the thin tail of $-7 \pm 10 \text{ rad m}^{-2}$. We tried to check the consistency of the values for the foreground polarized intensity and polarization angle, but were not able, due to the relatively weak depolarization signatures in the thin-tail structures, to solve simultaneously (using the approach of Wolleben & Reich) for the RM and the foreground parameters.

5. DISCUSSION

5.1. Evidence in Faraday Rotation of the Shell of DeHt 5

Given the west-southwest projected space velocity of the DeHt 5 central star, WD 2218+706, we might expect to see evidence in the optical image (Figure 1) and radio polarization images (Figure 2) of a bow shock at the south-west edge of the disk of the PN. A close connection between enhanced optical emission and Faraday rotation is observed at the leading edge of at least one other old PN (Sh 2-216; Ransom et al. 2008). Since, however, both enhanced optical emission and Faraday rotation rely on column density of ionized material, and a large component of the space velocity of DeHt 5 lies along the line of sight (see § 2.1), a leading-edge enhancement may appear in projection more like a ring for DeHt 5. Moreover, recent hydrodynamic simulations of the interaction with the ISM of moderately fast-moving PNe ($50\text{--}100 \text{ km s}^{-1}$) show that “hot spots” in the nebular shell migrate over time downstream from the leading-edge of the interaction, and sit in the more advanced stages of the PN-ISM interaction at approximately the halfway point between the upstream and downstream sides of the shell (see Wareing et al. 2007a). If this is the case for the $\gtrsim 90,000$ yr-old DeHt 5 (see Table 1), then the column density of ionized material in the projected ring would be higher than for any other location in the PN.

There is no indication of a ring in Figure 1, or in any other narrow-band or spectral-line optical image of DeHt 5 (see Tweedy & Kwitter 1996). We return to this point at the end of this subsection. There is, however, evidence for a ring-like structure in the radio polarization images. The bent structure on the disk of DeHt 5 (see, in particular, Figure 4b) may be the outline of a ring which forms a clear boundary with the surrounding regions on the north-east (arc) and south (ridge) sides. Indeed, a circular ring, aligned in three-dimensions perpendicular to the space velocity of DeHt 5, would have a projected shape on the front side (i.e., the side closest to Earth) similar to that formed by the arc and ridge. (We show in Figure 5 a two-dimensional slice through the ring described here on a plane perpendicular to the plane of the sky.) Furthermore, close inspection of the west and north-west edges of the disk in both polarized intensity and polarization angle shows that there is a jagged, though very narrow, transition between the plateau and off-source region. There are three

reasons why the ring boundary on the west side may be more subtle than that on the east side: (1) The polarization angle difference between the plateau and thick tail (immediately east of the disk) is larger than that between the plateau and off-source region immediately west of the disk. A smaller mean off-source to on-source rotation results in a lesser degree of beam depolarization, and consequently a thinner and more subtle boundary. (2) There may be spherical (or circular in the case of a ring) asymmetries in the density of material in the shell (Wareing et al. 2007a,b). (3) Spatial variations in the strength and/or orientation of the magnetic field at the back (west) side of the ring may be smaller in magnitude than those on the front (east) side. We elaborate on the magnetic field geometry in the shell of DeHt 5 below.

We estimate in the plateau region between the ridge and arc a mean RM of $+19 \pm 11 \text{ rad m}^{-2}$. Since no estimate is given in the literature for the electron density in the shell of DeHt 5, we cannot derive (see eq. [2]) the magnitude of the line-of-sight magnetic field in the plateau. However, the sign of the RM indicates that the field in this central region is directed out of the plane of the sky. If the field is ISM in origin (e.g., Ransom et al. 2008), we can explain simultaneously the out-of-the-sky component near the center of the disk of DeHt 5 and the into-the-sky component discussed in § 5.3 for the thick tail (see Figure 5): The intrinsic ISM field in the region about DeHt 5 (see § 5.3) is deflected around the shell of DeHt 5 by the fast-moving PN system, such that a small out-of-the-sky component is generated near the center of the disk of DeHt 5. The rapid spatial change of the deflected field at the east edge of the disk provides one ingredient for the beam depolarization responsible for the arc. The other ingredient is the ionized material in the front portion of the enhanced ring. A similar deflection and enhancement at the bottom of the shell of DeHt 5 may be responsible for the appearance of the ridge.

The narrow-band and spectral-line optical emission for DeHt 5 show no clear leading edge or ring-like enhancements. Indeed, the only enhanced emission seen at optical wavelengths is the filamentary emission at the north edge of the disk. Some authors (e.g., Tweedy & Kwitter 1996; Parker et al. 2006) suggest that the diffuse optical emission on the disk of DeHt 5 may be ionized ISM, and speculate that the PN shell has long since dissipated. In contrast, the radio polarization results for both the disk and the thick tail (see § 5.2) indicate that DeHt 5, though certainly towards the ends of its evolution, is still a PN. Polarimetric observations have the advantage over total-intensity observations of being very sensitive to small spatial changes in electron density and/or magnetic-field orientation, specifically those at the projected boundary between the evolved shell and the off-source region.

5.2. Two Distinct Tails in the Wake of DeHt 5?

Are the Faraday-rotation structures behind DeHt 5 really the signatures of a tail of ionized material deposited downstream by the interaction between DeHt 5 (and its progenitor) and the ISM? Could the structures in fact trace the history of the interaction first between the AGB wind and the ISM (thin tail) and second between the PN and the previously established AGB-ISM interaction zone (thick tail)? We look in § 5.2.1 at evidence favoring interpretation of the thick tail as the product of material stripped during the more recent PN-ISM interaction, and in § 5.2.2 at evidence supporting interpretation of the thin tail as the outcome of stripping during the preceding AGB-ISM interaction.

5.2.1. Evidence of the PN-ISM tail

The most compelling pieces of evidence that the $\sim 0.5^\circ \times \sim 0.3^\circ$ Faraday-rotation structure is the signature of a PN-ISM tail is its north-east side attachment to DeHt 5 and the approximate alignment of its major axis with the projected space velocity of WD 2218+706. It is very unlikely that a line-of-sight Faraday-rotation structure, unrelated to DeHt 5, would have one end bounded by DeHt 5, and extend away from DeHt 5 in the direction from which WD 2218+706 came. But why then is the alignment approximate, and not exact to within the error bars of the projected space velocity?

There are two reasons why the position angle of the major axis of the thick tail might differ by $21.5^\circ \pm 2.5^\circ$ from that of the projected space velocity of WD 2218+706. First, the measured proper motion of WD 2218+706 may not represent that of the system. Both the HST (Benedict et al. 2009) and USNO (Harris et al. 2007) observations of WD 2218+706 show signs of a binary companion. Using the example provided by Benedict et al. (2009), an M1 V star would be at the limit of detectability if separated from WD 2218+706 by 5.2 AU. The resulting 11 yr orbital period for this system would result in a transverse velocity as high as 14 km s^{-1} (assuming an orbital eccentricity of zero). If the transverse orbital motion were approximately perpendicular to the system proper motion, the position angle of the projected (instantaneous) motion of WD 2218+706 would differ from that of the system motion by $\sim 18^\circ$. A more massive K8 V star with a separation of just 3.2 AU would also be at the limit of detectability (see Table 8 in Benedict et al. 2009), and would give a maximum position-angle difference of $\sim 21^\circ$. Second, the system may be accelerating toward a massive, extended molecular cloud complex. The cloud runs $\sim 10^\circ$ from $(l = 100^\circ, b = 13^\circ)$ to $(l = 117^\circ, b = 22^\circ)$, and contains $\sim 6 \times 10^4 M_\odot$ of material (see Grenier et al. 1989). (The elongated feature which runs diagonally across the top-right portion of Figure 3 may be the Faraday-rotation signature of this extensive cloud.) Distance estimates for the cloud range

between ~ 300 pc (Grenier et al. 1989) and ~ 400 pc (Bally & Reipurth 2001), indicating that this mass is in the same region of the local arm as DeHt 5. We elaborate more on the gravitational effect of the molecular cloud on WD 2218+706 (and its progenitor) in § 5.2.2 below.

In addition to its location and alignment, the $\sim 0.5^\circ$ major-axis length of the thick tail may itself provide evidence that this region is the PN-ISM tail of DeHt 5. At a distance of 345 ± 20 pc, the angular length of the thick tail corresponds to a projected physical length of ~ 3.0 pc. If we assume, for the moment, that the material in the thick tail is stationary with respect to the ambient ISM, then the 45.8 ± 2.4 km s $^{-1}$ projected velocity of WD 2218+706 leads to an age for the PN-ISM interaction of $\sim 64,000$ yr. This value represents a lower limit, since stripped material will not instantaneously decelerate to zero velocity. The simulations of Wareing et al. (2007c) for the interaction between the Mira system and the ISM give a velocity lag for the tail material of just 10–15 km s $^{-1}$, but point out that the viscosity in the tail may be underestimated. Taking the minimum value for the lag in the DeHt 5 tail to be ~ 10 km s $^{-1}$, we derive an upper limit for the interaction age of $\sim 380,000$ yr. Since the PN-ISM interaction is expected to start $\lesssim 10,000$ yr after the onset of the PN phase for fast-moving systems (see Wareing et al. 2007a), the thick-tail length suggests that DeHt 5 is between 74,000 and 390,000 yr old. The kinematic age for DeHt 5 is 87,000 yr (see Table 1), close to the lower limit of this range. In quite some contrast, observational estimates of the mass, effective temperature, and luminosity of WD 2218+706 (see Benedict et al. 2009) suggest a post-AGB age for the transitioning star of $\gtrsim 300,000$ yr (see evolutionary tracks in Schönberner & Blöcker 1996), a value much closer to the upper limit. Wareing et al. (2007a) suggest that the kinematic age underestimates the true age for a PN interacting with the ISM, since nebular expansion has ceased at the leading edge of the interaction.

The $\sim 0.3^\circ$ width of the thick tail is also consistent with the simulations of Wareing et al. (2007a), which show, for systems moving at speeds of 50–75 km s $^{-1}$, a PN-ISM tail width ~ 2 times the diameter of the PN shell. However, the ISM magnetic field should also be taken into account in estimating the width of the ionized tail. In the case of an ISM field oriented roughly parallel to the direction of motion, expansion of the tail material may be restricted. In the opposite case, i.e., a field oriented perpendicular to the direction of motion (see § 5.3), expansion may be facilitated. A full magnetohydrodynamic (MHD) simulation of the PN-ISM interaction could more clearly establish the role of the ISM magnetic field in the evolution of the tail’s morphology. The small beam-sized knots in the thick tail signify regions of enhanced turbulence, and are consistent with simulations which show that ~ 0.1 pc vortices can be shed downstream from the leading edge of the PN-ISM interaction (see Wareing et al. 2007b).

5.2.2. Evidence of the AGB-ISM tail

If we accept that the thick tail is the signature of the PN-ISM interaction for DeHt 5, then the best evidence that the thin tail is the signature of the earlier AGB-ISM interaction is its relative position behind, and approximate alignment with, the thick tail. Again, the approximate alignment requires some explanation. The three Faraday-rotation structures which make up the $\sim 1.8^\circ$ thin tail fall on a line with position angle $\sim 45^\circ$ (north of east). This line is $\sim 13^\circ$ more northerly than the major axis of the thick tail. The orbit we computed for WD 2218+706 (see § 2.1) gives a straight-line trajectory for the star over the past ~ 2 Myr. However, the orbit takes into account only the global Galactic potential, and not the contributions of close encounters with large masses such as the molecular cloud complex described above in § 5.2.1. If the cloud is < 100 pc distant, the resulting acceleration would, over ~ 1 Myr, increase the westward velocity of the star system by $\sim 20 \text{ km s}^{-1}$, yielding the curved trajectory between the thin and thick tails seen in Figure 3. Indeed, such an acceleration would simultaneously explain the difference in position angles between the thin and thick tails and between the thick tail and projected space velocity of WD 2218+706.

At a distance of 345 ± 20 pc, the $\sim 1.8^\circ$ angular length of the thin tail corresponds to a projected physical length of ~ 11.0 pc. Allowing the same range of velocities for the thin tail material as for the thick tail material, we find lower and upper limits for the age of the apparent AGB-ISM interaction of 0.23 Myr and 1.4 Myr. The upper limit is roughly consistent with the lifetime in the thermally-pulsing AGB (TP-AGB) phase for a star with metallicity similar to the Sun and final core mass similar to the estimated mass of WD 2218+706 (see Bloeker 1995b). However, with seven or more thermal pulses predicted for the full TP-AGB phase (e.g., Vassiliadis & Wood 1993), we might expect a less disjointed Faraday-rotation signature in the thin tail than actually observed (see also the simulations of Wareing et al. 2007c). On the other hand, models suggest that mass loss is most intense (for stars with initial mass $< 2.5 M_\odot$) during the later stages of the TP-AGB phase, specifically the last 2–3 thermal-pulse cycles (Vassiliadis & Wood 1993; Marigo & Girardi 2007). Indeed, the recent models of Marigo & Girardi (2007) show that the mass-loss rates are a factor 2 or more higher for the last 2–3 pulses, and give a period for the final pulse cycles of 0.1–0.2 Myr. If the thin tail is the signature of the later stages of the TP-AGB phase, then the three-component Faraday-rotation structure suggests a time frame of 0.3–0.6 Myr, consistent with the low end of the range suggested by the tail’s full length. A direct measurement of the velocity of the gas in the thin tail would help to put observational constraints on the models.

5.3. Mass Ejected During the PN-ISM Interaction

Based on the evidence and consistencies described in § 5.2.1, we believe that the thick tail seen in the radio polarization images is the Faraday-rotation signature of material strewn downstream by the interaction between DeHt 5 and the ISM. Since we have an estimate of the RM in the thick tail (see § 4.2), we can derive (via eq. [2]) the electron density, and therefore mass, in the strewn material. To estimate the path length through the thick tail, we approximate the tail as a cylinder with cross-sectional diameter equal to its projected semi-minor axis ($\sim 0.3^\circ$ or ~ 1.8 pc). The mean path length through the thick tail is then $\Delta l_{\text{av}} \approx 1.4$ pc. Since there is no direct measurement of the ISM magnetic field in the region around DeHt 5, we take for the nominal strength of the field the average azimuthal value given by Heiles (1996): $4.2 \mu\text{G}$. In the local arm, this field points toward $l = 84^\circ \pm 4^\circ$ (see Brown & Taylor 2001). At the midpoint of the thick tail ($l = 111.3^\circ$), the azimuthal field points into the sky, consistent with the sign of the RM , and makes a $27^\circ \pm 4^\circ$ angle with the line of sight (see Figure 5). Considering the range of possible combinations of the regular and random components of the Galactic magnetic field (see, e.g., Ransom et al. 2008) along this line, we estimate an uncertainty in the azimuthal field strength of $1.3 \mu\text{G}$. With these values, we derive for the line-of-sight component of the ISM field in the region of the thick tail $B_{\parallel} = 3.7 \pm 1.3 \mu\text{G}$.⁶ Since the azimuthal field lies largely perpendicular to the direction of motion, and the material in the thick tail is ionized (see below), the field is likely pulled forward slightly inside the tail creating a “magnetic wake” (see Figure 5). The result of this magnetic wake is a field that has on the near (i.e., Earth-facing) side of the thick tail a line-of-sight component smaller than the intrinsic field, and on the far side a line-of-sight component larger than the intrinsic field. The net effect for our purposes, assuming minimal compression of the field lines within the tail, is a mean line-of-sight component essentially the same as that quoted above for the intrinsic azimuthal field. Using $RM = -15 \pm 5 \text{ rad m}^{-2}$, $\Delta l_{\text{av}} \approx 1.4$ pc, and $B_{\parallel} = 3.7 \pm 1.3 \mu\text{G}$, we derive for the electron density in the thick tail $n_e = 3.6 \pm 1.8 \text{ cm}^{-3}$.

The gas in the thick tail is likely completely ionized (see Wareing et al. 2007a). Under this assumption, the number density for protons in the thick tail is the same as that for electrons: $n_{\text{H}} = 3.6 \pm 1.7 \text{ cm}^{-3}$. Using a cylindrical volume for the thick tail, with length ~ 3.0 pc and cross-sectional diameter ~ 1.8 pc, we estimate the total number of hydrogen ions in the thick tail to be $(8.1 \pm 4.0) \times 10^{56}$. This value corresponds to a total mass of $0.68 \pm 0.33 M_{\odot}$. If we assume that the ambient density in the region surrounding DeHt 5 is

⁶We used the midpoints of the thick tail in longitude and latitude to project the azimuthal field onto the line of sight. Note that, at a distance of 345 ± 20 pc, the thick tail sits ~ 70 pc above the Galactic plane, well within the predicted ~ 1.2 -kpc scale height for the Galactic magnetic field (Han & Qiao 1994).

$n_{\text{H}} \sim 1 \text{ cm}^{-3}$, then the mass ejected into the thick tail during the PN-ISM interaction stage is $0.49 \pm 0.33 \text{ M}_{\odot}$.

5.4. Mass Ejected During the AGB-ISM Interaction

Using the estimate of the mean RM given in § 4.3, we can derive the total ionized mass in the three components which define the thin tail. If the thin tail is indeed the signature of the later stages of the AGB-ISM interaction, then the ionized mass content places a lower limit (see below) on the mass ejected during the TP-AGB phase. Since the uncertainty in the RM for the thin-tail components is quite large, we use only the nominal value ($RM \sim -7 \text{ rad m}^{-2}$) for the following derivation, and caution the reader to view the given ionized mass value as only a first estimate.

To estimate the path length through the thin tail, we approximate each component as a sphere with diameter equal to its projected diameter ($\sim 0.3^{\circ}$ or $\sim 1.8 \text{ pc}$). The mean path length through the thin tail is then $\Delta l_{\text{av}} \approx 1.2 \text{ pc}$. The azimuthal ISM field (see § 5.3) makes a 28° angle with the line of sight at the midpoint of the thin tail ($l = 112.4^{\circ}$), yielding $B_{\parallel} \approx 3.6 \mu\text{G}$. Using $RM \sim -7 \text{ rad m}^{-2}$, $\Delta l_{\text{av}} \approx 1.2 \text{ pc}$, and $B_{\parallel} \approx 3.6 \mu\text{G}$, we derive for the electron density in each of the thin-tail components $n_e \sim 2.0 \text{ cm}^{-3}$.

In contrast to the thick tail, the material in the thin tail is likely only partially ionized. (The ionization fraction is difficult to estimate, since we have no independent knowledge of the ionization age or density of the thin tail material.) Thus, we can consider the electron density to be only a lower limit on the mass density in the thin-tail components: $n_{\text{H}} \gtrsim 2.0 \text{ cm}^{-3}$. Using a spherical volume with diameter $\sim 1.8 \text{ pc}$ for each component, we estimate the total number of hydrogen ions/atoms in the thin tail to be $\gtrsim 5.4 \times 10^{56}$. This value corresponds to a total mass of $\gtrsim 0.45 \text{ M}_{\odot}$. The mass ejected into the thin tail during the AGB-ISM interaction stage is $\gtrsim 0.23 \text{ M}_{\odot}$, based on an ambient density of $n_{\text{H}} \sim 1 \text{ cm}^{-3}$.

5.5. Possible Implications of the DeHt 5 Tails

The stripped-mass estimates given above for the thick ($0.49 \pm 0.33 \text{ M}_{\odot}$) and thin ($\gtrsim 0.23 \text{ M}_{\odot}$) tails, though subject to some important assumptions and (especially for the thin tail) large uncertainties, indicate that a significant amount of material, originally in the envelope of the WD 2218+706 progenitor, has been deposited downstream. This result is consistent with hydrodynamic simulations (Villaver et al. 2003; Wareing et al. 2007a), and has implications for (1) the PN missing-mass problem, and (2) models which describe the

impact of the deaths of intermediate-mass stars on the ISM. We discuss each of these briefly below.

Observations show that, on average, only $0.15 M_{\odot}$ of material is present in ionized form in the shells of PNe (see, e.g., Zhang 1995). For intermediate-mass stars with initial masses in the $1\text{--}3 M_{\odot}$ range (i.e., an initial mass for which a final core mass similar to that of WD 2218+706 is plausible), this nebular mass represents $\lesssim 40\%$ of the mass lost during AGB and post-AGB evolution (e.g., Bloeker 1995a). The “missing” $\gtrsim 60\%$ may be partly in neutral form within the PN (see Aaquist & Kwok 1991), but the majority is likely in the tails of material ejected during AGB-ISM and PN-ISM interactions. Future radio polarimetric observations of the tail regions of DeHt 5 and other PNe may yield mass estimates accurate enough to account for all of the progenitor mass loss, and eliminate altogether the missing-mass problem for PNe.

PNe are much smaller than SNRs: compare ~ 2.5 pc for the average diameter of an old PNe (Tweedy & Kwitter 1996) to ~ 30 pc for the average diameter of a Galactic SNR (Kothés et al. 2006). In a one-to-one comparison, an SNR has ~ 1730 times the volume of a PN. If all of the mass lost by intermediate-mass stars were ultimately “trapped” within the shells of their PNe, then the influence of intermediate-mass stars on the composition and dynamics of the ISM would indeed be negligible compared to their high-mass counterparts. The observations presented here for DeHt 5, however, as well as those presented elsewhere for the Mira system and Sh 2-188, show that the volume of influence for intermediate-mass stars is much greater than a PN shell. The thick tail behind DeHt 5 has a volume ~ 9 times that of the PN. Taking into account also the thin tail, the volume ratio of tail to PN shell increases to ~ 21 . If the tails behind DeHt 5 are representative of those behind other PNe, then the contrast between the volume of the ISM influenced by the death of an intermediate-mass star and that of a high-mass star is somewhat reduced. Furthermore, since intermediate-mass stars complete several orbits of the Galactic center, and oscillate on their orbits up and down through the Galactic plane, many regions of the Galactic ISM may have been touched by their dynamically active tails. A detailed model, which takes into account the initial mass function as well as lifetimes and trajectories of disk stars, is necessary in order to fully assess the relative importance of the deaths of intermediate and high-mass stars in the Galactic ISM.

6. CONCLUSIONS

Here we give a summary of our results and conclusions:

1. We have presented 1420 MHz polarization images for the $5^\circ \times 5^\circ$ region around the PN DeHt 5.

2. Narrow Faraday-rotation structures trace approximately the north-east (arc) and south (ridge) edges of the disk of DeHt 5. These narrow features may represent an enhanced ring of material in the shell of DeHt 5, which is aligned in three-dimensions perpendicular to the space velocity of the white dwarf central star, WD 2218+706.

3. A small region of relatively high polarized intensity (plateau) sits at approximately the midpoint of the disk of DeHt 5. We have estimated via comparison of on-source and off-source polarization angles a RM through the plateau of $+18 \pm 12 \text{ rad m}^{-2}$. The positive sense for the RM indicates that the magnetic field in the plateau is directed out of the sky.

4. A Faraday-rotation structure, $\sim 3 \text{ pc}$ long and $\sim 1.8 \text{ pc}$ wide, runs away from the north-east edge of DeHt 5 in a direction roughly opposite that of the sky-projected space velocity of the system. Based on its location and alignment, as well as consistencies with hydrodynamic simulations (Villaver et al. 2003; Wareing et al. 2007a), we conclude that the structure is the signature of ionized material ram-pressure stripped and deposited downstream during a $> 74,000 \text{ yr}$ interaction between DeHt 5 and the ISM. We call this structure the “thick tail” to distinguish it from the more subtle tail-like structure summarized in points 8–9 below.

5. We have estimated, using the approach of Wolleben & Reich (2004), a RM through the thick tail of $-15 \pm 5 \text{ rad m}^{-2}$. The negative sense for the RM indicates that the magnetic field is directed into the sky.

6. We have presented a qualitative model which interprets the into-the-sky magnetic field in the region of the thick tail as the large-scale azimuthal field of the Galaxy. The out-of-the-sky magnetic field near the center of the disk of DeHt 5 (see point 3 above) is naturally explained in this model as the deflected and compressed azimuthal field.

7. With the RM given above (point 5), we have estimated the electron density in the thick tail to be $n_e = 3.6 \pm 1.8 \text{ cm}^{-3}$. Assuming that the ambient density in the region surrounding DeHt 5 is $n_H \sim 1 \text{ cm}^{-3}$, the mass ejected into the thick tail during the PN-ISM interaction is $0.49 \pm 0.33 \text{ M}_\odot$.

8. A series of three roughly circular Faraday-rotation structures appear behind the thick tail, and have a collective length of $\sim 11.0 \text{ pc}$. These structures, which we call the “thin tail,” may be the signature of the earlier interaction between the WD 2218+706 progenitor and the ISM. The AGB-ISM interaction is predicted by hydrodynamic simulations, and has been clearly observed for one system (Mira AB; see Martin et al. 2007). If the thin tail behind

DeHt 5 is indeed the signature of the AGB-ISM interaction, then this is the first time that both the PN-ISM and AGB-ISM interactions have been observed for the same source.

9. We have estimated via comparison of on-source and off-source polarization angles a RM through the thin tail of $\sim -7 \text{ rad m}^{-2}$. With this value for the RM , we have estimated the total ionized mass in the thick tail to be $\sim 0.45 M_{\odot}$. Assuming, again, that the ambient density is $n_{\text{H}} \sim 1 \text{ cm}^{-3}$, the mass ejected into the thin tail during the $>0.23 \text{ Myr}$ AGB-ISM interaction is $\gtrsim 0.23 M_{\odot}$. (We give a lower limit since the thin tail is likely only partially ionized.) Targeted, polarimetric observations at multiple frequencies between 1 and 3 GHz would yield a more precise estimate of the RM in the thin-tail components, and allow for a more rigorous derivation of the mass content.

10. The discovery of the tails representing the PN-ISM and possibly the AGB-ISM interactions for DeHt 5 (and its progenitor) has important implications for the PN missing-mass problem and models which describe the impact of the deaths of intermediate-mass stars on both the composition and dynamics of the ISM. Future radio polarimetric observations of other old PNe and late-stage AGB stars may provide additional insight.

ACKNOWLEDGMENTS. We thank the anonymous referees for constructive reviews of the paper and for comments helpful in the preparation of the final manuscript. RRR thanks the Dean of Science, Technology, and Health at Okanagan College for arranging release time for research. The Canadian Galactic Plane Survey is a Canadian project with international partners, and has been supported by a grant from NSERC. The Dominion Radio Astrophysical Observatory is operated as a national facility by the National Research Council of Canada. This research is based in part on observations with the 100-m telescope of the MPIfR at Effelsberg. The Second Palomar Observatory Sky Survey (POSS-II) was made by the California Institute of Technology with funds from the National Science Foundation, the National Geographic Society, the Sloan Foundation, the Samuel Oschin Foundation, and the Eastman Kodak Corporation.

REFERENCES

- Aaquist, O. B. & Kwok, S. 1991, *ApJ*, 378, 599
- Bally, J. & Reipurth, B. 2001, *ApJ*, 552, L159
- Bannister, N. P., Barstow, M. A., Holberg, J. B., & Bruhweiler, F. C. 2001, in *Astronomical Society of the Pacific Conference Series*, Vol. 226, 12th European Workshop on White Dwarfs, ed. J. L. Provencal, H. L. Shipman, J. MacDonald, & S. Goodchild, 105–+

- Barstow, M. A., Bannister, N. P., Holberg, J. B., Hubeny, I., Bruhweiler, F. C., & Napiwotzki, R. 2001, *MNRAS*, 325, 1149
- Benedict, G. F., Mc Arthur, B. E., Napiwotzki, R., Harrison, T. E., Harris, H. C., Nelan, E., Bond, H. E., Patterson, R. J., & Ciardullo, R. 2009, *AJ*, 138, 1969
- Bloecker, T. 1995a, *A&A*, 299, 755
- . 1995b, *A&A*, 297, 727
- Borkowski, K. J., Sarazin, C. L., & Soker, N. 1990, *ApJ*, 360, 173
- Brown, J. C. & Taylor, A. R. 2001, *ApJ*, 563, L31
- Dauphole, B. & Colin, J. 1995, *A&A*, 300, 117
- Dehnen, W. & Binney, J. J. 1998, *MNRAS*, 298, 387
- Good, S. A., Barstow, M. A., Burleigh, M. R., Dobbie, P. D., & Holberg, J. B. 2005, *MNRAS*, 364, 1082
- Gray, A. D., Landecker, T. L., Dewdney, P. E., Taylor, A. R., Willis, A. G., & Normandeau, M. 1999, *ApJ*, 514, 221
- Grenier, I. A., Lebrun, F., Arnaud, M., Dame, T. M., & Thaddeus, P. 1989, *ApJ*, 347, 231
- Han, J. L. & Qiao, G. J. 1994, *A&A*, 288, 759
- Harris, H. C., Dahn, C. C., Canzian, B., Guetter, H. H., Leggett, S. K., Levine, S. E., Luginbuhl, C. B., Monet, A. K. B., Monet, D. G., Pier, J. R., Stone, R. C., Tilleman, T., Vrba, F. J., & Walker, R. L. 2007, *AJ*, 133, 631
- Haverkorn, M., Gaensler, B. M., McClure-Griffiths, N. M., Dickey, J. M., & Green, A. J. 2006, *ApJS*, 167, 230
- Heiles, C. 1996, in *Astronomical Society of the Pacific Conference Series*, Vol. 97, *Polarimetry of the Interstellar Medium*, ed. W. G. Roberge & D. C. B. Whittet, 457–+
- Johnson, D. R. H. & Soderblom, D. R. 1987, *AJ*, 93, 864
- Kerber, F., Furlan, E., Rauch, T., & Roth, M. 2000, in *Astronomical Society of the Pacific Conference Series*, Vol. 199, *Asymmetrical Planetary Nebulae II: From Origins to Microstructures*, ed. J. H. Kastner, N. Soker, & S. Rappaport, 313–+
- Kerber, F., Guglielmetti, F., Mignani, R., & Roth, M. 2002, *A&A*, 381, L9

- Kerber, F., Mignani, R. P., Guglielmetti, F., & Wicenec, A. 2003, *A&A*, 408, 1029
- Kothes, R., Fedotov, K., Foster, T. J., & Uyaniker, B. 2006, *A&A*, 457, 1081
- Landecker, T. L., Dewdney, P. E., Burgess, T. A., Gray, A. D., Higgs, L. A., Hoffmann, A. P., Hovey, G. J., Karpa, D. R., Lacey, J. D., Prowse, N., Purton, C. R., Roger, R. S., Willis, A. G., Wyslouzil, W., Routledge, D., & Vaneldik, J. F. 2000, *A&AS*, 145, 509
- Landecker, T. L., Reich, W., Reid, R. I., Reich, P., Wolleben, M., Kothes, R., Uyaniker, B., Gray, A. D., Del Rizzo, D., Furst, E., Taylor, A. R., & Wielebinski, R. 2010, *ArXiv e-prints*
- Lawson, K. D., Mayer, C. J., Osborne, J. L., & Parkinson, M. L. 1987, *MNRAS*, 225, 307
- Marigo, P. & Girardi, L. 2007, *A&A*, 469, 239
- Martin, D. C., Seibert, M., Neill, J. D., Schiminovich, D., Forster, K., Rich, R. M., Welsh, B. Y., Madore, B. F., Wheatley, J. M., Morrissey, P., & Barlow, T. A. 2007, *Nature*, 448, 780
- Matthews, L. D., Libert, Y., Gérard, E., Le Bertre, T., & Reid, M. J. 2008, *ApJ*, 684, 603
- Napiwotzki, R. 1999, *A&A*, 350, 101
- Napiwotzki, R. & Schoenberger, D. 1995, *A&A*, 301, 545
- Parker, Q. A., Acker, A., Frew, D. J., Hartley, M., Peyaud, A. E. J., Ochsenbein, F., Phillipps, S., Russeil, D., Beaulieu, S. F., Cohen, M., Köppen, J., Miszalski, B., Morgan, D. H., Morris, R. A. H., Pierce, M. J., & Vaughan, A. E. 2006, *MNRAS*, 373, 79
- Ransom, R. R., Uyaniker, B., Kothes, R., & Landecker, T. L. 2008, *ApJ*, 684, 1009
- Reich, P. & Reich, W. 1988, *A&A*, 196, 211
- Reich, W., Fürst, E., Reich, P., Uyaniker, B., Wielebinski, R., & Wolleben, M. 2004, in *The Magnetized Interstellar Medium*, ed. B. Uyaniker, W. Reich, & R. Wielebinski, 45–50
- Roger, R. S., Costain, C. H., Landecker, T. L., & Swerdlyk, C. M. 1999, *A&AS*, 137, 7
- Schönberger, D. & Blöcker, T. 1996, *Ap&SS*, 245, 201
- Simmons, J. F. L. & Stewart, B. G. 1985, *A&A*, 142, 100

- Soker, N. & Dgani, R. 1997, *ApJ*, 484, 277
- Taylor, A. R., Gibson, S. J., Peracaula, M., Martin, P. G., Landecker, T. L., Brunt, C. M., Dewdney, P. E., Dougherty, S. M., Gray, A. D., Higgs, L. A., Kerton, C. R., Knee, L. B. G., Kothes, R., Purton, C. R., Uyaniker, B., Wallace, B. J., Willis, A. G., & Durand, D. 2003, *AJ*, 125, 3145
- Tweedy, R. W. & Kwitter, K. B. 1996, *ApJS*, 107, 255
- Uyaniker, B., Landecker, T. L., Gray, A. D., & Kothes, R. 2003, *ApJ*, 585, 785
- Vassiliadis, E. & Wood, P. R. 1993, *ApJ*, 413, 641
- Villaver, E., García-Segura, G., & Manchado, A. 2003, *ApJ*, 585, L49
- Wareing, C. J., O’Brien, T. J., Zijlstra, A. A., Kwitter, K. B., Irwin, J., Wright, N., Greimel, R., & Drew, J. E. 2006a, *MNRAS*, 366, 387
- Wareing, C. J., Zijlstra, A. A., & O’Brien, T. J. 2007a, *MNRAS*, 382, 1233
- . 2007b, *ApJ*, 660, L129
- Wareing, C. J., Zijlstra, A. A., O’Brien, T. J., & Seibert, M. 2007c, *ApJ*, 670, L125
- Wareing, C. J., Zijlstra, A. A., Speck, A. K., O’Brien, T. J., Ueta, T., Elitzur, M., Gehrz, R. D., Herwig, F., Izumiura, H., Matsuura, M., Meixner, M., Stencel, R. E., & Szczerba, R. 2006b, *MNRAS*, 372, L63
- Wolleben, M., Landecker, T. L., Reich, W., & Wielebinski, R. 2006, *A&A*, 448, 411
- Wolleben, M. & Reich, W. 2004, *A&A*, 427, 537
- Xilouris, K. M., Papamastorakis, J., Paleologou, E., & Terzian, Y. 1996, *A&A*, 310, 603
- Zhang, C. Y. 1995, *ApJS*, 98, 659

Table 1. Properties of DeHt 5 and its Central Star WD 2218+706

| Parameter | Value | Reference |
|---------------------------------------|----------------------------|-----------|
| Nebula Properties | | |
| Angular Diameter (arcmin) | 9 | 1 |
| Linear Diameter (pc) | 0.90 ± 0.05^a | 1 4 |
| Kinematic Age (yrs) | 87000^b | 2 4 |
| Central Star Properties | | |
| Equatorial Coordinates (J2000) | 22 19 33.713, +70 56 03.28 | 3 |
| Galactic Coordinates (deg) | 111.093, +11.641 | 3 |
| Trigonometric Parallax (mas) | 2.90 ± 0.15^c | 4 |
| Distance (pc) | 345^{+19}_{-17} | 4 |
| Proper Motion (mas yr ⁻¹) | 21.93 ± 0.12^d | 4 |
| Radial Velocity (km s ⁻¹) | -40.9 ± 1.5 | 5 |
| Spectral Classification | DA ^e | 6 |
| T_{eff} (K) | 76500 ± 5800^f | 2 |
| Mass (M _⊙) | 0.57 ± 0.02 | 4 |

Note. — Units of right ascension are hours, minutes, and seconds, and units of declination are degrees, arcminutes, and arcseconds; mas \equiv milliarcseconds.

^aThe linear diameter reflects the angular diameter given by Tweedy & Kwitter (1996) and the trigonometric parallax given by Benedict et al. (2009).

^bThe kinematic age estimate is adjusted from Napiwotzki (1999) to the trigonometric parallax given by Benedict et al. (2009).

^cEstimate given is the weighted average of estimates from the Hubble Space Telescope (HST) and the United States Naval Observatory (USNO; see Harris et al. 2007).

^dEquatorial components for the proper motion: $\mu_\alpha = -11.80 \pm 0.10$, $\mu_\delta = -18.49 \pm 0.08$ mas yr⁻¹.

^eA DAO classification is used in some references, since trace amounts of helium are present in the photosphere (see Barstow et al. 2001).

^f T_{eff} estimates in the literature range between 57400 K (Barstow et al. 2001) and 76500 K (Napiwotzki 1999).

References. — 1. Tweedy & Kwitter 1996; 2. Napiwotzki 1999; 3. Kerber et al. 2003; 4. Benedict et al. 2009; 5. Good et al. 2005; 6. Napiwotzki & Schoenberner 1995.

Table 2. On-Source and Off-Source Polarized Intensities and Polarization Angles

| Region (1) | P.A. ($^{\circ}$) (2) | $\sigma_{\text{P.A.}}$ ($^{\circ}$) (3) | P.I. K (4) | $\sigma_{\text{P.I.}}$ K (5) | n (6) |
|---------------------------------|-------------------------------|---|------------------|------------------------------------|------------|
| —————Disk Features————— | | | | | |
| Ridge | −74 | 15 | 0.103 | 0.044 | 410 |
| Arc | −86 | 12 | 0.081 | 0.039 | 325 |
| Plateau (between Ridge and Arc) | −29 | 9 | 0.252 | 0.045 | 140 |
| —————Tails————— | | | | | |
| Thick | −72 | 8 | 0.162 | 0.055 | 2800 |
| Thick (excl. knots) | −66 | 6 | 0.182 | 0.039 | 1650 |
| Thin | −55 | 6 | 0.260 | 0.048 | 2600 |
| —————Off-Source————— | | | | | |
| Disk/Thick | −48 | 6 | 0.297 | 0.047 | 21500 |
| Thin | −48 | 6 | 0.309 | 0.047 | 14000 |

Note. — Col. (1) See text for description of ridge, arc, plateau, thick tail, and thin tail. Off-source (Disk/Thick) refers to all pixels of the $1^{\circ} \times 1^{\circ}$ region centered on DeHt 5 (see Figure 2 or Figure 3) that are outside the disk of DeHt 5 and not in the thick tail. Off-source (Thin) refers to all pixels within 0.5° of the thin tail (see Figure 3), but not in the thin tail. Col. (2) Mean polarization angle in the respective region. (Note that polarization angles are modulo 180° ; i.e., angles of -90° and $+90^{\circ}$ are equivalent.) Col. (3) Standard deviation in polarization angle. Col. (4) Mean polarized intensity in the respective region. Col. (5) Standard deviation in polarized intensity. Col. (6) Number of pixels used to estimate the mean polarization angle and polarized intensity.

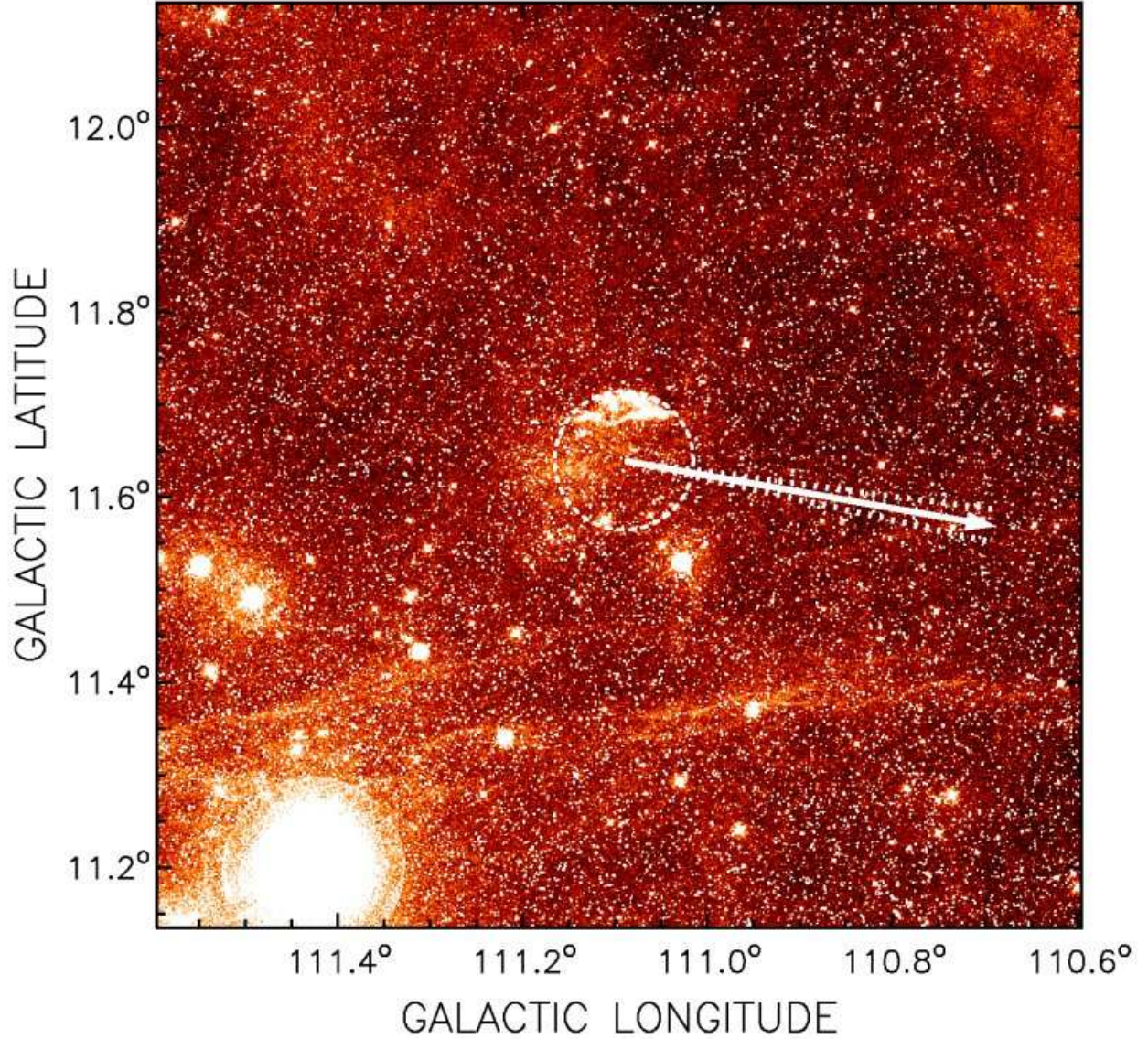


Fig. 1.— R-band DSS optical image of a $1^\circ \times 1^\circ$ region centered on the position of WD 2218+706, the central star of PN DeHt 5 (see Table 1). Here and hereafter, images are presented in Galactic coordinates, with Galactic north up and Galactic east to the left. The intensity scale is in photon counts with lighter shades indicating higher counts. The range of intensities has been adjusted to highlight extended emission. The angular resolution is $\sim 1''$. The dashed circle drawn on the image, and on each subsequent image, shows the approximate extent of the “visible disk” (see § 2) of DeHt 5. The solid arrow and adjacent dotted lines on the image, and on the images presented in Figs. 2 and 3, indicate the projected space velocity and space-velocity error cone of WD 2218+706. The length of the solid arrow represents the change in the sky position of WD 2218+706 over the next $\approx 50,000$ yrs. The filamentary structure at the northernmost edge of DeHt 5 is also given the designation LBN 538. The bright star in the south-east corner of the image is HR 8557 ($m_V = 5.5$).

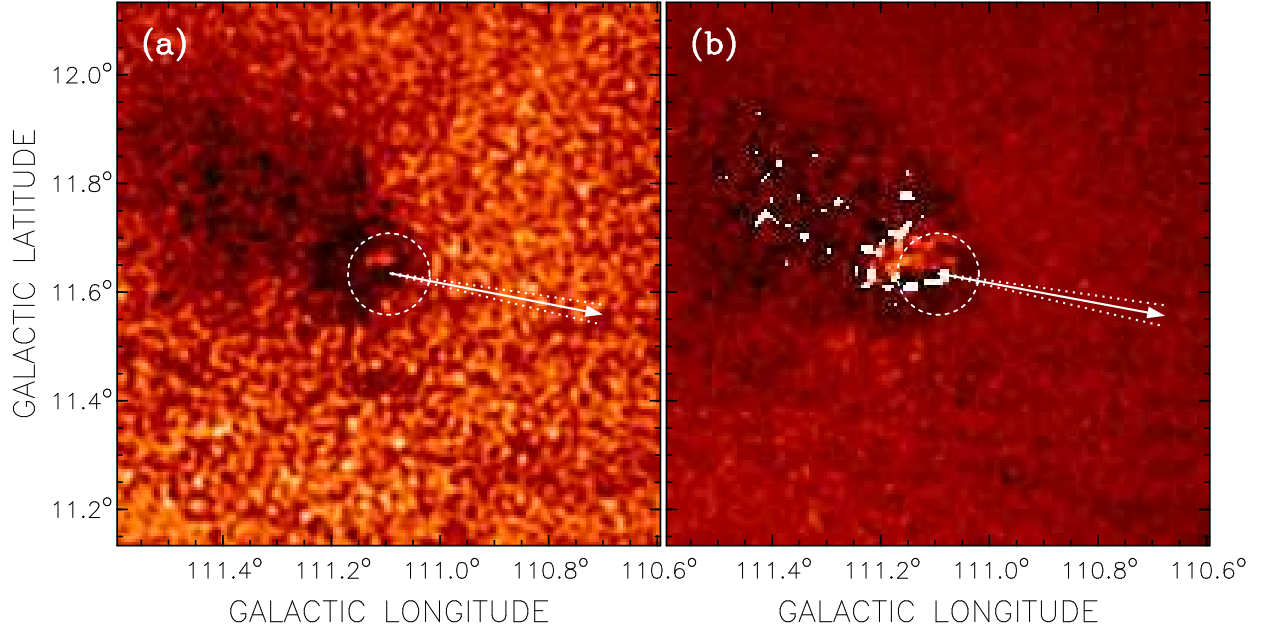


Fig. 2.— Images at 1420 MHz in (a) polarized intensity, $P = \sqrt{Q^2 + U^2 - (1.2\sigma)^2}$, and (b) polarization angle, $\theta_P = \frac{1}{2} \arctan U/Q$ of the same $1^\circ \times 1^\circ$ region presented in Fig. 1. The intensity scale is in brightness temperature in (a) and runs from 0 to 0.63 K, with lighter shades indicating higher temperatures. The intensity scale in (b) extends from -90° (black) to $+90^\circ$ (white). Note that abrupt black-to-white transitions in (b) do not represent large changes in angle, since polarization angles of -90° and $+90^\circ$ are equivalent. The resolving beam at the center of each image is $1.17' \times 1.11'$ (full-width at half-maximum; FWHM) oriented at a position angle (east of north) of -50° . The resolving beam varies in size over each image by $\sim 3\%$.

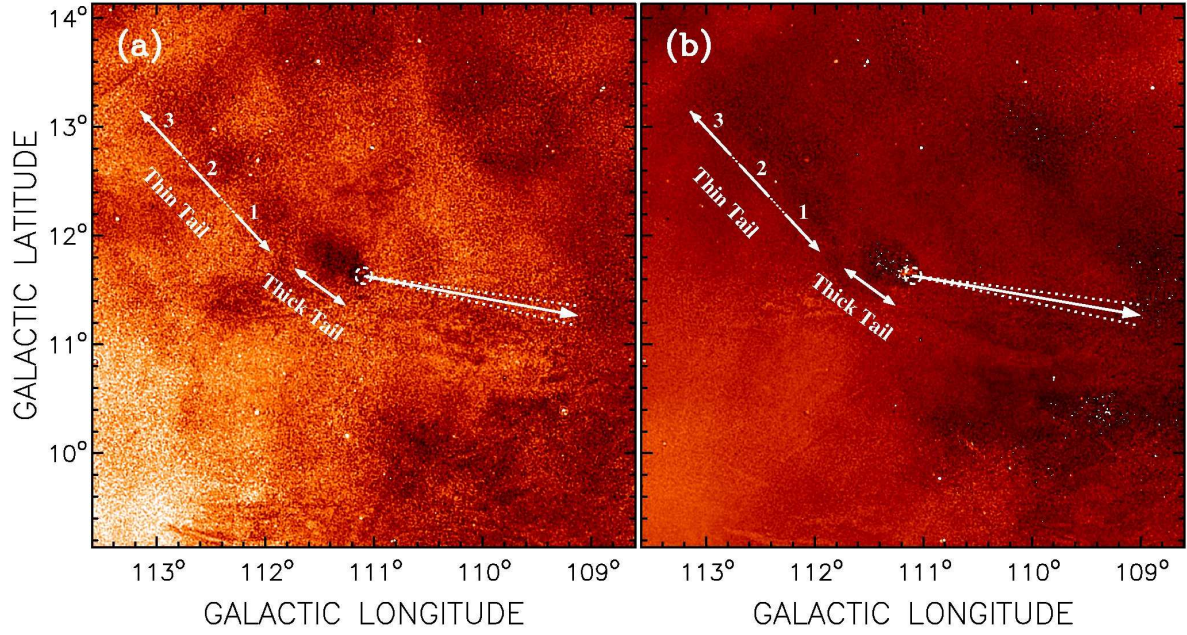


Fig. 3.— Images at 1420 MHz in (a) polarized intensity and (b) polarization angle for a $5^\circ \times 5^\circ$ region around DeHt 5. The intensity scales are as described in Fig. 2. The approximate extents of the thick and thin tails described in the text are indicated. The three regions comprising the thin tail are labeled 1–3, with the numbers increasing with distance from DeHt 5. The length of the solid arrow represents (at this scale) the change in the sky position of WD 2218+706 over the next $\approx 250,000$ yrs.

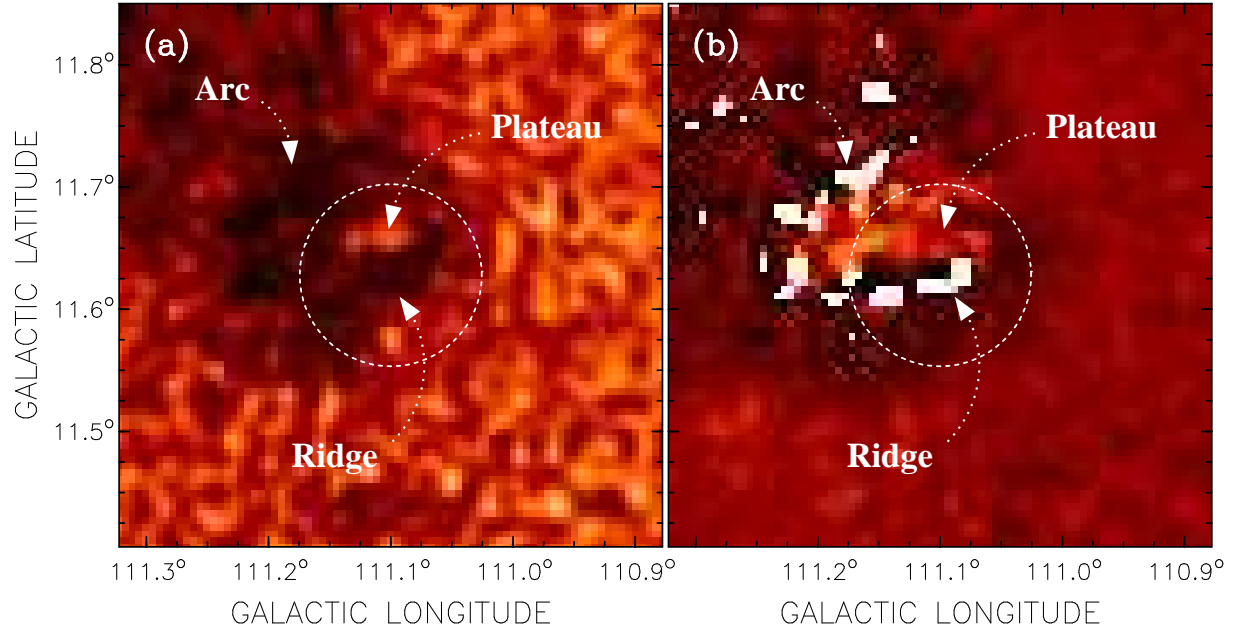


Fig. 4.— (a) Polarized intensity and (b) polarization angle images zoomed-in to a $0.4^\circ \times 0.4^\circ$ region around DeHt 5. The intensity scales are as described for Fig. 2. The disk features discussed in the text are labeled.

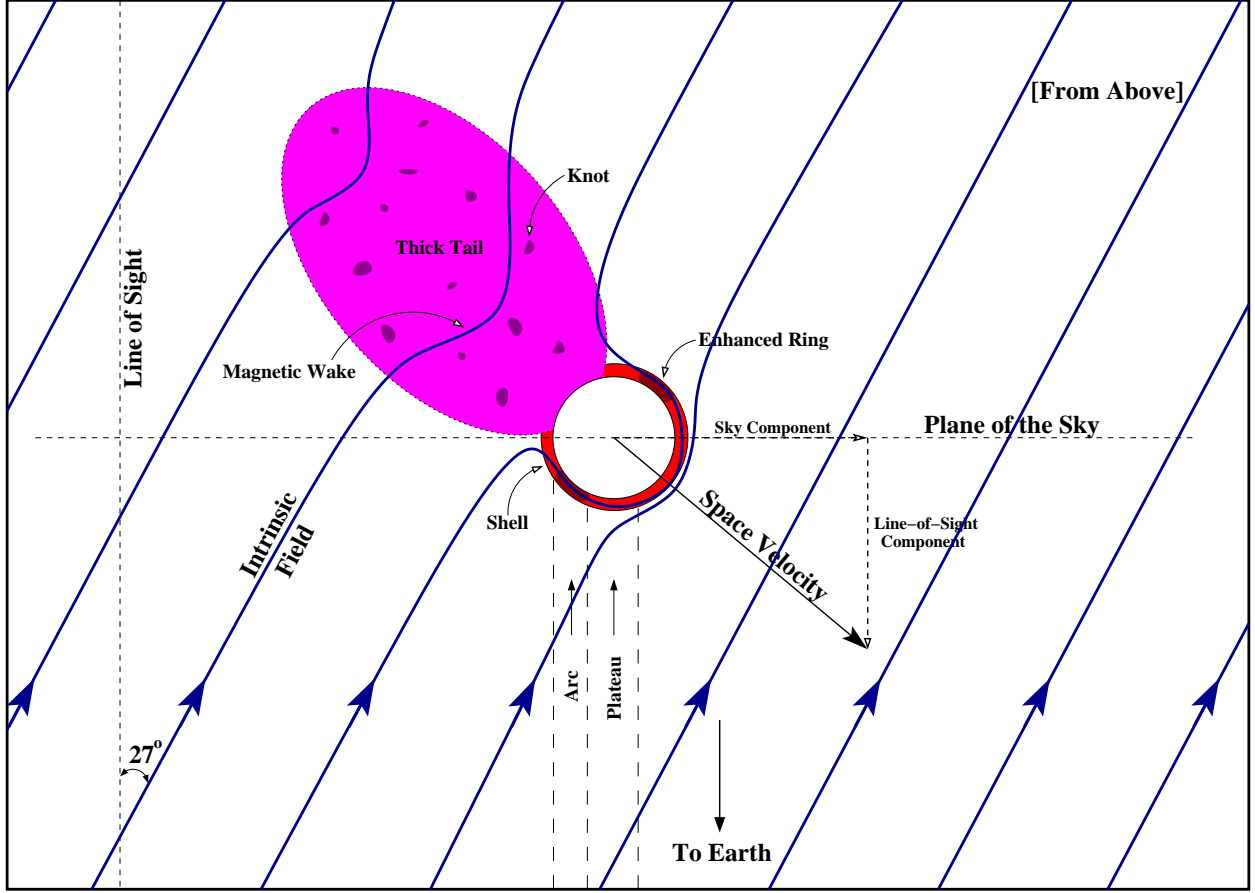


Fig. 5.— Qualitative model showing the interaction between DeHt 5 and the magnetized ISM. The perspective is that of an observer sitting well above the Galactic plane and looking down on the center of DeHt 5 (with Galactic east to the left). The space velocity of WD 2218+706, projected onto a plane parallel to the Galactic plane, is indicated, with line-of-sight and sky components. The intrinsic ISM magnetic field is inclined $\approx 27^\circ$ relative to the line of sight. The field lines immediately surrounding DeHt 5 are compressed and deflected around the leading edge of the shell of the PN. The deflection leads to a field which has a rapidly varying line-of-sight component on the east side of the disk (Arc) and a more uniform orientation, with small out-of-the-sky component, near the center of the disk (Plateau). Note that the arc is coincident with the front-side of the Enhanced Ring, which is oriented roughly perpendicular to the space velocity (see § 5.1). The ~ 3 -pc-long Thick Tail, representing ionized material stripped at the interface between DeHt 5 and the ISM during the PN phase, deflects the intrinsic field in the direction of motion (Magnetic Wake), but not to the same extent as the dense PN shell. We have drawn the thick tail on this plane such that its major axis is aligned with the space velocity of WD 2218+706. The small misalignment that we see in the radio polarization images may lie completely in the plane of the sky.